



TITLE:

The molecular mechanism of photochemical internalization of cell penetrating peptide-cargo-photosensitizer conjugates.

AUTHOR(S):

Ohtsuki, Takashi; Miki, Shunya; Kobayashi, Shouhei;
Haraguchi, Tokuko; Nakata, Eiji; Hirakawa, Kazutaka;
Sumita, Kensuke; Watanabe, Kazunori; Okazaki, Shigetoshi

CITATION:

Ohtsuki, Takashi ...[et al]. The molecular mechanism of photochemical internalization of cell penetrating peptide-cargo-photosensitizer conjugates.. Scientific reports 2015, 5: 18577.

ISSUE DATE:

2015-12-21

URL:

<http://hdl.handle.net/2433/216044>

RIGHT:

This work is licensed under a Creative Commons Attribution 4.0 International License. The images or other third party material in this article are included in the article's Creative Commons license, unless indicated otherwise in the credit line; if the material is not included under the Creative Commons license, users will need to obtain permission from the license holder to reproduce the material. To view a copy of this license, visit <http://creativecommons.org/licenses/by/4.0/>

SCIENTIFIC REPORTS

OPEN

The molecular mechanism of photochemical internalization of cell penetrating peptide-cargo-photosensitizer conjugates

Takashi Ohtsuki¹, Shunya Miki¹, Shouhei Kobayashi², Tokuko Haraguchi², Eiji Nakata³, Kazutaka Hirakawa⁴, Kensuke Sumita¹, Kazunori Watanabe¹ & Shigetoshi Okazaki⁵

Received: 01 October 2015
Accepted: 23 November 2015
Published: 21 December 2015

In many drug delivery strategies, an inefficient transfer of macromolecules such as proteins and nucleic acids to the cytosol often occurs because of their endosomal entrapment. One of the methods to overcome this problem is photochemical internalization, which is achieved using a photosensitizer and light to facilitate the endosomal escape of the macromolecule. In this study, we examined the molecular mechanism of photochemical internalization of cell penetrating peptide-cargo (macromolecule)-photosensitizer conjugates. We measured the photophysical properties of eight dyes (photosensitizer candidates) and determined the respective endosomal escape efficiencies using these dyes. Correlation plots between these factors indicated that the photogenerated $^1\text{O}_2$ molecules from photosensitizers were highly related to the endosomal escape efficiencies. The contribution of $^1\text{O}_2$ was confirmed using $^1\text{O}_2$ quenchers. In addition, time-lapse fluorescence imaging showed that the photoinduced endosomal escape occurred at a few seconds to a few minutes after irradiation (much longer than $^1\text{O}_2$ lifetime), and that the pH increased in the endosome prior to the endosomal escape of the macromolecule.

The therapeutic efficacy of many drug delivery strategies is often limited by the inefficient transfer of cargo macromolecules such as proteins and nucleic acids to the cytosol consequential to their endosomal entrapment^{1,2}. One of the methods to overcome this problem is to use a photosensitizer and light to facilitate the endosomal escape of the macromolecules^{3–8}, termed photochemical internalization (PCI). It has been considered that in this technique, the endosomes are disrupted by reactive oxygen species generated photo-dependently from photosensitizers^{9–12}. However, the correlations between endosomal escape efficiency and the photosensitizing reactions of various photosensitizers have not been systematically examined. Thus, the properties of photosensitizers important for PCI need to be clarified through the use of multiple photosensitizers.

To analyze the mechanism of PCI, a photosensitizing RNA carrier molecule was used in this study. This carrier molecule can bind to an RNA and deliver it into a cell by the PCI strategy, whereby the carrier/RNA complexes are first entrapped within endosomes, and then photo-dependently escape the endosomes. The photosensitizing RNA carrier molecule consists of a photosensitizer and TatU1A, a fusion protein of HIV TAT-derived cell-penetrating peptide (CPP) and human U1A-derived RNA-binding protein^{13–15}. An advantage to the use of a photosensitizer attached to the TatU1A protein for studying the PCI mechanism is that the localization of photosensitizers (~1 kDa) is strongly affected by the larger protein moiety (~16 kDa). Thus, the difference of intrinsic “cellular localization” among various photosensitizers can virtually be ignored, and focus can be placed on the “photosensitizing reaction” of the photosensitizers.

In this study, we measured the photophysical properties of eight dyes as photosensitizer candidates, and investigated which property is most related to effective photoinduced endosomal disruption using TatU1A-dye

¹Department of Medical Bioengineering, Okayama University, 3-1-1 Tsushima-naka, Okayama 700-8530, Japan.

²Advanced ICT Research Institute Kobe, NICT, 588-2 Iwaoka, Iwaoka-cho, Nishi-ku, Kobe 651-2492, Japan. ³Institute of Advanced Energy, Kyoto University, Gokasho, Uji, Kyoto 611-0011, Japan. ⁴Department of Applied Chemistry and Biochemical Engineering, Graduate School of Engineering, Shizuoka University, Johoku 3-5-1, Naka-ku, Hamamatsu 432-8561, Japan. ⁵Department of Medical Spectroscopy, Hamamatsu University School of Medicine, 1-20-1 Handayayama, Higashi-ku, Hamamatsu, 431-3192, Japan. Correspondence and requests for materials should be addressed to T.O. (email: ohtsuk@okayama-u.ac.jp)

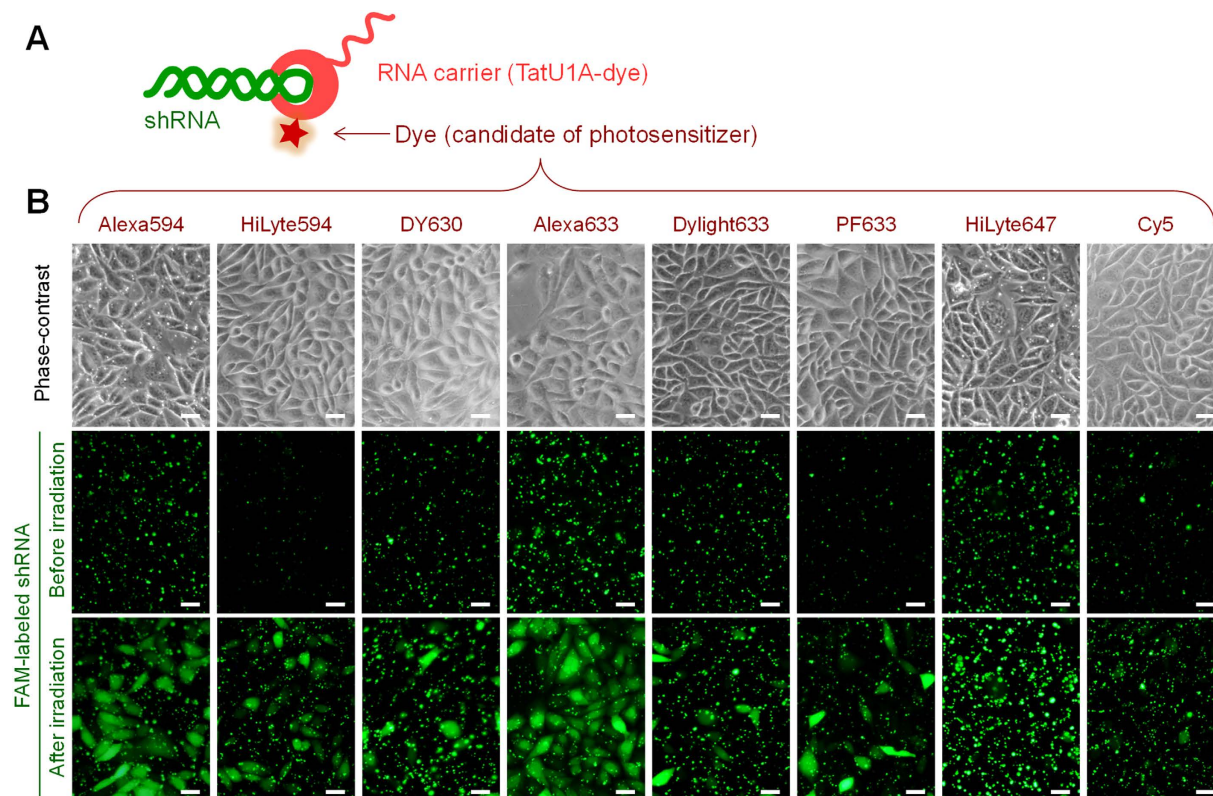


Figure 1. Photoinduced RNA internalization by CHO cells. (A) Complex of the RNA carrier-TatU1A-dye with FAM-labeled short hairpin RNA (shRNA). (B) Phase contrast and FAM fluorescence images of the cells after incubation with TatU1A-dye/FAM-labeled RNA complex and followed by photostimulation. Scale bars indicate 20 μ m.

(TatU1A-photosensitizer) conjugates. The fluorescence quantum yield (ϕ) and $^1\text{O}_2$ quantum yield (ϕ_Δ) were measured as the photophysical dye properties. In addition, the photo-dependent heat generation efficiency was approximately estimated by the parameter $(1 - \phi - \phi_\Delta)$. The influence of $^1\text{O}_2$ quenchers was utilized to investigate the PCI mechanism. Furthermore, time-lapse images of the photoinduced endosomal disruption events were analyzed.

Results

Photo-dependent cytosolic RNA internalization using various TatU1A-dyes. Various TatU1A-dye conjugates (Fig. 1A) were used to attempt cellular RNA delivery and photoinduced cytoplasmic dispersion (or endosomal escape) of the RNA. Eight dyes, that absorb yellow to red light (550–650 nm), were used as candidates for photosensitizers for the PCI strategy. Since these dyes can be excited by similar excitation wavelengths, endosomal escape efficiencies using these dyes were compared under the same photostimulation conditions (wavelength, light intensity, and irradiation time) (Table 1). Photo-dependent cytoplasmic dispersion of the RNA was efficiently induced with TatU1A-Alexa633 and TatU1A-Alexa594 (Fig. 1B), indicating that these dyes can work as photosensitizers when they are attached to the TatU1A protein. In contrast, several dyes, such as DyLight 633 and Cy5, induced only minimal photo-dependent endosomal RNA escape.

Contributions of the photophysical properties of the dyes to endosomal escape. To identify the key characteristics of the dyes that contribute to photo-dependent endosomal escape of the cargo RNA, we investigated the phenomena after excitation of the dyes by light. The major phenomena after dye excitation are fluorescence emission, heat generation, and $^1\text{O}_2$ generation. First, the $^1\text{O}_2$ quantum yields (ϕ_Δ) of these dyes were estimated by measuring the near-infrared phosphorescence of $^1\text{O}_2$ at around 1270 nm. Photoinduced $^1\text{O}_2$ generation from the dyes was detected for some dyes upon being dissolved in 1-octanol (Table 1), though this was hardly detected in water, probably because of the weak phosphorescence of $^1\text{O}_2$ in water. Octanol, having a long hydrophobic carbon chain with a small hydrophilic hydroxyl group, seems to provide an environment similar to that in membrane lipids. The relative extent of $^1\text{O}_2$ photogenerated from each photosensitizer in the endosomal escape experiment was estimated by the formula $[\phi_\Delta \times \text{Ef}]$, in which Ef is the efficacy of excitation of each photosensitizer. The $[\phi_\Delta \times \text{Ef}]$ value was highly correlated with the endosomal escape efficiencies of TatU1A-dye/RNA complexes ($R^2 = 0.79$) (Fig. 2a), indicating that photoinduced $^1\text{O}_2$ generation from dyes is required for endosomal escape of the dye-conjugate molecules.

In contrast, the relative extent of the fluorescence quantum yield of each dye in octanol did not significantly correlate with the endosomal escape efficiency of the TatU1A-dye/RNA complex ($R^2 < 0.5$) (Fig. 2B). The fluorescence

Dye	Singlet oxygen quantum yield (φ_{Δ})	Fluorescence quantum yield (φ)	$1 - \varphi - \varphi_{\Delta}$	Endosomal escape efficiency (%)
Alexa Fluor 594	0.028	0.922	0.050	60.6 ± 6.3
HiLyte Fluor 594	0.006	0.628	0.366	32.9 ± 7.3
DY 630	0.011	0.170	0.819	22.9 ± 4.3
Alexa Fluor 633	0.043	0.706	0.251	86.6 ± 3.9
DyLight 633	0.005	0.060	0.935	10.6 ± 1.6
Promo Fluor 633	0.012	0.305	0.683	24.8 ± 3.7
HiLyte Fluor 647	0.007	0.362	0.631	11.6 ± 1.8
Cy5	0.009	0.464	0.527	11.4 ± 2.8

Table 1. Singlet oxygen quantum yield (φ_{Δ}), fluorescence quantum yield (φ), and $[1 - \varphi - \varphi_{\Delta}]$ of each dye in octanol, and photoinduced endosomal RNA escape efficiency with each TatU1A-dye. *Photo-dependent heat generation efficiency.

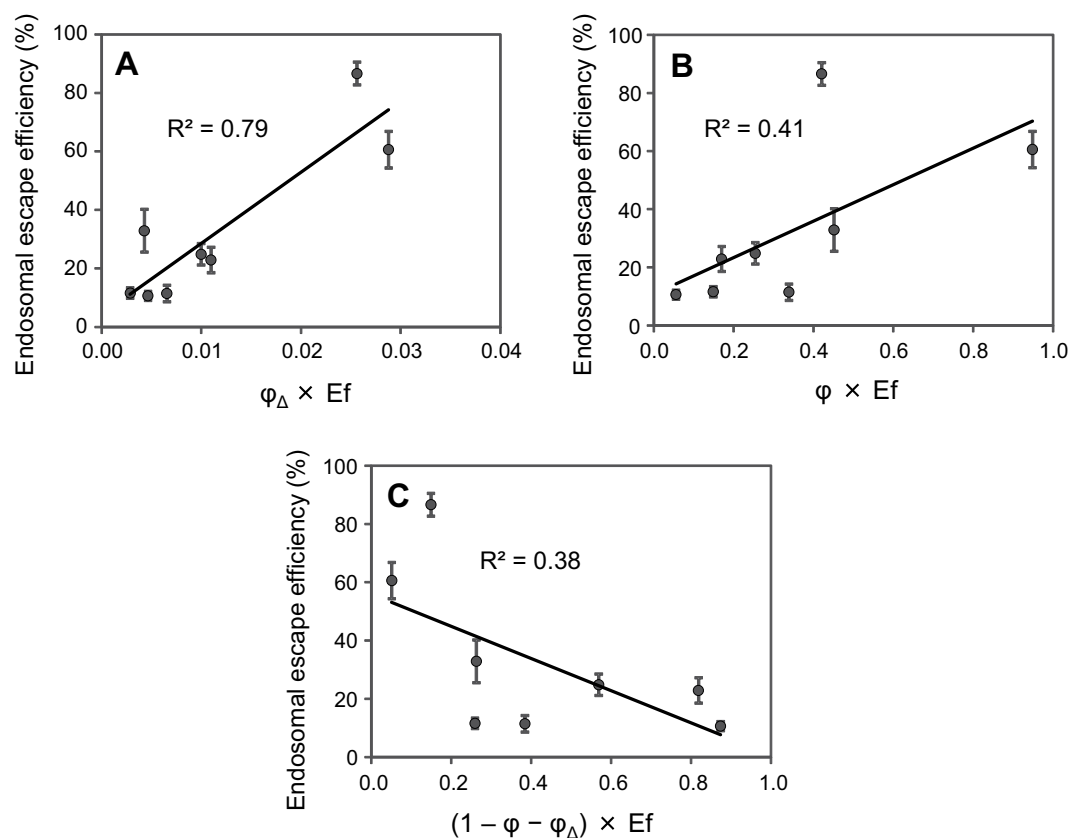


Figure 2. Relationship between endosomal escape and photophysical parameters of phorosensitizers. Correlations between photoinduced endosomal escape efficiencies of the TatU1A-dye/RNA complexes and $[\varphi_{\Delta} \times Ef]$ (A), $[\varphi \times Ef]$ (B), or $[(1 - \varphi - \varphi_{\Delta}) \times Ef]$ (C) of each dye. The φ_{Δ} and φ values were measured in octanol. Data represent means ± SD, n = 5.

quantum yield of each dye in water also did not correlate with the endosomal escape efficiency (Supplementary Fig. S1A).

After excitation of these dyes, the absorbed light energy would be used mainly for fluorescence, 1O_2 generation, and heat generation. Since phosphorescence was not detected from these dyes, the value $[1 - (\text{fluorescence quantum yield } \varphi) - (\text{singlet oxygen quantum yield } \varphi_{\Delta})]$ is likely to represent a kind of quantum yield for heat, that is, $[\text{heat energy generated from a dye}]/[\text{total light energy absorbed by the dye}]$. To consider the contribution of heat generation from dyes, the correlation between $[(1 - \varphi - \varphi_{\Delta}) \times Ef]$ and the endosomal escape efficiency was evaluated. Figure 2C shows that there was no significant correlation between these measures, suggesting that heat generated from dyes does not contribute significantly to the endosomal escape of the carrier/RNA complex. These results (Fig. 2) indicate that photo-dependent endosomal escape is most highly related to 1O_2 among the three major phenomena (fluorescence, heat, and 1O_2) occurring after dye excitation.

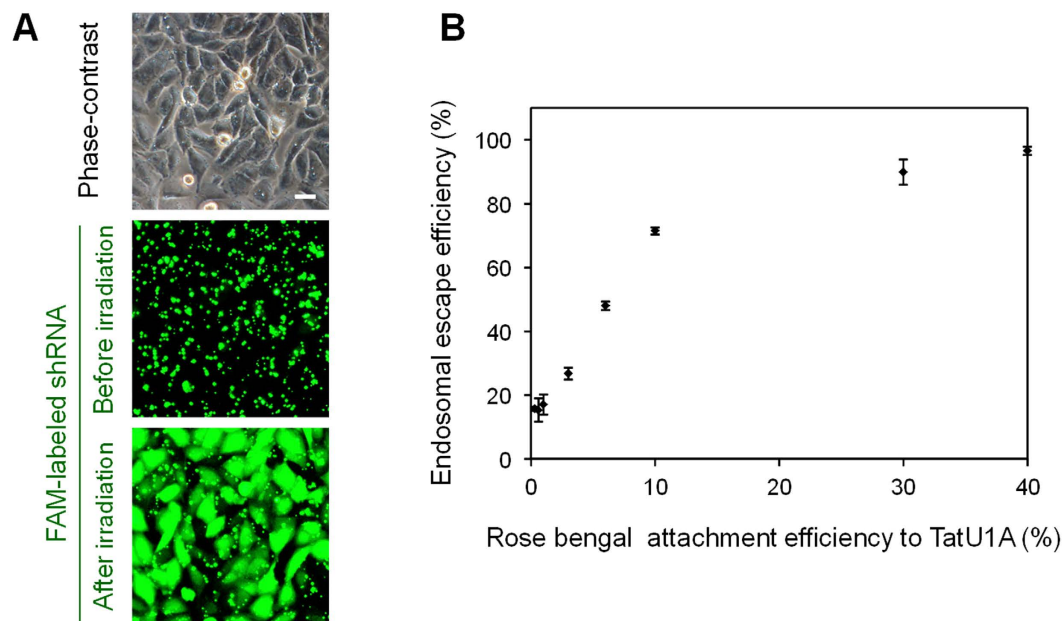


Figure 3. PCI using the TatU1A-rose bengal/RNA complex. (A) Photoinduced endosomal escape of the FAM-labeled shRNA using TatU1A-rose bengal (rose bengal attachment efficiency was 30%). Scale bars indicate 20 μ m. (B) Correlation between the photoinduced endosomal escape efficiency of the TatU1A-rose bengal/RNA complex and the rate of attachment of rose bengal to TatU1A. To induce endosomal escape, the cells were irradiated at 530–550 nm, 930 mW/cm² for 11 s. Data represent means \pm SD, n = 3.

We note that the majority of reported PCI experiments have utilized photosensitizers that were not covalently attached to carrier-cargo complexes^{5–7,16–18}. In contrast, in this study, we examined a photosensitizer that was covalently linked to the carrier protein. If this study had been performed using unlinked photosensitizers, we could not have concluded that only the photoinduced ¹O₂ generation of the photosensitizers was important to effect endosomal escape of the cargo, because endosomal escape efficiency must also be affected by the specific cellular localization of each photosensitizer. However, here the influence of the localization was minimized through the use of photosensitizers attached to a protein that always delivers each photosensitizer into endosomes.

PCI using TatU1A-rose bengal and a shRNA cargo molecule. To further investigate the contribution of photoinduced ¹O₂ generation to endosomal escape, we performed PCI using TatU1A-rose bengal and the FAM-labeled shRNA as the cargo molecule. Rose bengal is a well-known photosensitizer with a very high ¹O₂ quantum yield ($\varphi_{\Delta} = 0.86$ in EtOH¹⁹). We prepared several TatU1A-rose bengal conjugates with different rose bengal attachment efficiencies to the TatU1A protein (0–40%), and investigated the correlation between the attachment efficiency and endosomal escape efficiency. Photoinduced endosomal escape of the FAM-labeled shRNA using TatU1A-rose bengal was confirmed as shown in Fig. 3A. Figure 3B shows that the endosomal escape efficiency linearly correlated with the rose bengal attachment efficiency until the latter reached 10%. At greater attachment efficiencies, the endosomal escape efficiency approached a plateau. Since the light energy absorbed by rose bengal is primarily utilized for ¹O₂ generation, this result suggests that endosomal escape correlates to photoinduced ¹O₂ generation.

Influences of the ¹O₂ quenchers. To further confirm the contribution of ¹O₂, the influences of ¹O₂ quenchers on the endosomal escape efficiency were examined. We used two hydrophilic quenchers (histidine and NaN₃) and two lipophilic quenchers (α -tocopherol and crocetin). These ¹O₂ quenchers were added (i) with the same timing as the 2 h incubation with the TatU1A-Alexa633/RNA complex, or (ii) during the 1 h following complex incubation (Fig. 4, lower panel). All of the quenchers added at both times (i) and (ii) downregulated the endosomal escape efficiency of the TatU1A-Alexa633/RNA complex (Fig. 4). These results demonstrated significant correlation between photoinduced ¹O₂ generation and endosomal escape efficiency of the CPP-cargo-photosensitizer conjugate.

Imaging of photoinduced endosomal escape. To examine the mechanism of photoinduced endosomal cargo escape, time-lapse imaging was performed. In this experiment, CHO cells were treated with the complex of TatU1A-Alexa546 and FAM-labeled shRNA and then were photoirradiated. Time-lapse images of FAM-shRNA and TatU1A-Alexa546 after photoirradiation revealed that FAM fluorescence at the sites of endosomal dots increased with time (Fig. 5A, green arrows, and Fig. 5B) and then suddenly decreased to the original level within a few seconds (Fig. 5A,B, at 85–90 s). This rapid decrease in FAM fluorescence at the endosomal dot was always accompanied by the dispersion of FAM fluorescence into the cytosol, indicating that most of the FAM-labeled cargos were escaped from the disrupted endosomes. After the endosomal escape, the FAM fluorescence intensity in the disrupted endosome was almost the same as that in the surrounding area. Among the 204 disrupted endosomes, 151 (74%) were disrupted at 0–90 s after photoirradiation (Fig. 5C). Notably, the increase of FAM fluorescence

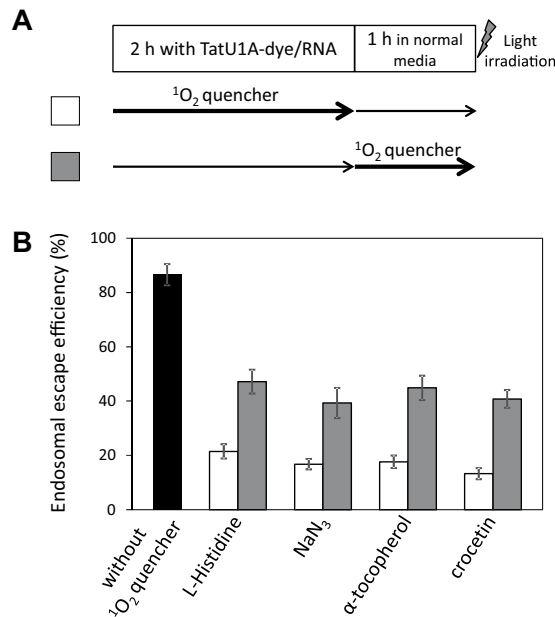


Figure 4. Influences of $^1\text{O}_2$ quenchers on endosomal escape efficiency. Each $^1\text{O}_2$ quencher was added to the cells simultaneous with (white bars) or subsequent to (gray bars) the treatment with the complex. The timing of $^1\text{O}_2$ quencher addition to the cells is shown in the lower panel. Data represent means \pm SD, $n = 3$.

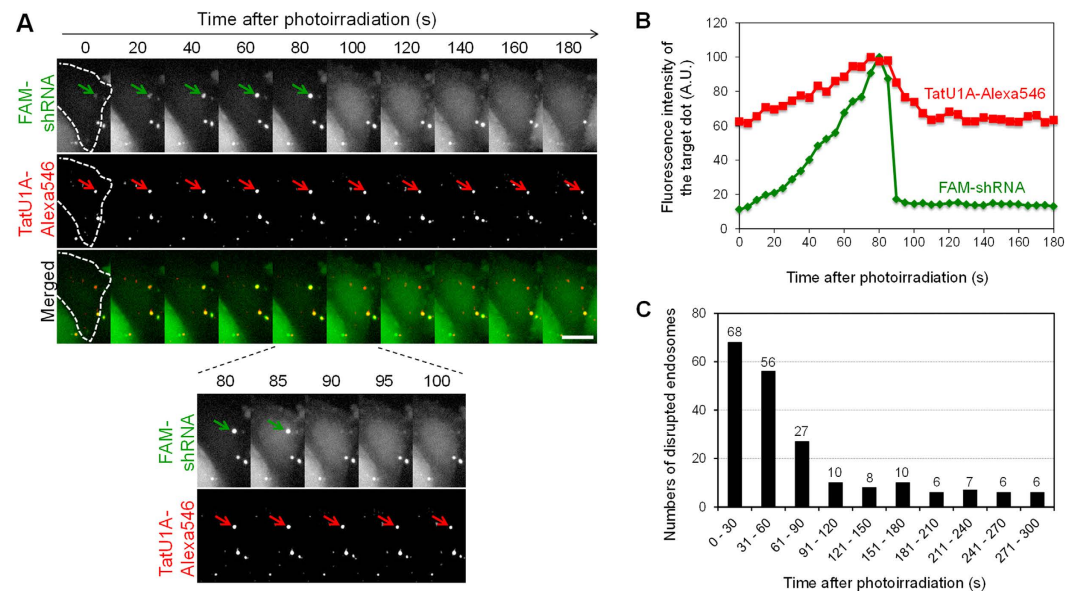


Figure 5. Time-lapse images and analyses of photoinduced endosomal disruption. (A) Time-lapse images of endosomal disruption after photoirradiation. The arrow shows the endosome that will be disrupted. Scale bars indicate $10\ \mu\text{m}$. (B) FAM and Alexa546 fluorescence intensities in the endosomes indicated by the arrows in (A). Background FAM or Alexa546 fluorescence intensity at the first time point (0 s) was subtracted from all data. Fluorescence intensities were normalized to the maximum fluorescence intensities of each of FAM and Alexa546. (C) Numbers of disrupted endosomes at each time after photoirradiation. In total, 204 endosomes in 159 cells were examined.

prior to endosome disruption was commonly observed for the endosomes which could be analyzed using a single particle tracking method ($n = 26$). We speculated that the increase of FAM fluorescence is most likely to indicate a pH increase in the endosome. The finding that the fluorescence of the FAM-labeled shRNA was much stronger at pH7.2 (which is similar to the cytosolic pH) than at pH5.5 (similar to the endosomal pH) (Supplementary Fig. S2) supports this notion.

In contrast to the FAM fluorescence, significant levels of Alexa546 fluorescence were still detected at the sites of the disrupted endosomes (Fig. 5A, red arrows, and Fig. 5B), indicating that most of the carrier molecules

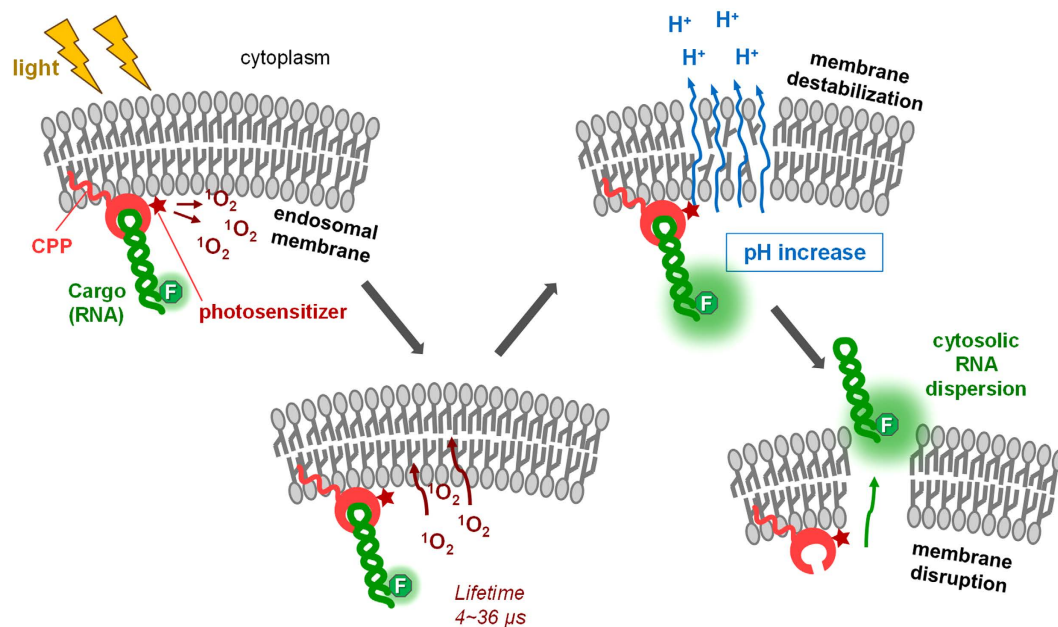


Figure 6. Schematic illustration of the endosomal disruption process using the cell penetrating peptide (CPP)-cargo-photosensitizer conjugate suggested by this study.

dissociated from the dispersed cargoes and remained at the original site of localization. This phenomenon might be partially explained by the fact that the Tat peptide has a strong affinity to endosomal membranes. It was recently reported that endosome disruption around exogenous materials triggers autophagy within about 5 min^{20,21}, with ubiquitinated proteins on the remnants of the disrupted endosomes being the plausible autophagy targets²². Thus, rapid dissociation of the cargoes from their carriers immediately after endosomal disruption might contribute the overall efficiency of cargo internalization into the cytosol in our present method.

Discussion

In this study, we investigated the molecular mechanism of photo-dependent endosomal disruption using CPP-cargo-photosensitizer conjugates. We employed eight dyes, such as Alexa Fluor 633 and DY630, as photosensitizers. These are not the photosensitizers used in most previous PCI studies, which utilized porphyrin-related molecules such as meso-tetraphenyl porphyrin disulphonate (TPPS_{2a})^{23–25}, disulfonated aluminum phthalocyanine (ALPcS_{2a})²⁶, and disulfonated tetraphenyl chlorin (TPCS_{2a}), the latter of which has been reported as a clinically suitable PCI photosensitizer²⁷. However, in this study, the photosensitizers were required to have a maleimide group for the reaction with the thiol group of the TatU1A protein, and at present, porphyrin photosensitizers with maleimide groups are not commercially available. Thus, eight commercially available dyes, which have similar excitation wavelengths to each other, were employed as photosensitizers in this study. Compared to porphyrin, the dyes used here are weak photosensitizers (*i.e.*, their ¹O₂ quantum yields are much lower than that of porphyrin). However, we demonstrated that certain of these weak photosensitizers could work effectively in PCI when attached to the Tat fusion protein.

Correlation plots between endosome escape efficiencies and the photophysical properties of each photosensitizer candidate indicated that the generated ¹O₂ from the photosensitizer was highly correlated to the endosomal escape efficiency. The ¹O₂ lifetime in lipid bilayers (12–36 μs)²⁸ differs from that in water (4.2 μs)²⁹. Therefore, the localization of photosensitizers affects the efficacy of the ¹O₂ produced. Photosensitizers might be located close to the membrane as presented in Fig. 6, or might also be partly embedded into the endosomal membranes to an extent depending on the chemical properties of the photosensitizers. However, in this study, the photosensitizers were not free, and the localizations of the photosensitizers must be highly affected by the linked TatU1A that is much larger than the photosensitizers themselves. Thus, the localizations of the individual photosensitizers are presumed to be similar. Furthermore, the difference between the lifetime of ¹O₂ generated near the membrane and that within the membrane seems to be diminished because ¹O₂ is likely to quickly enter and exit the membrane. The time to traverse a root mean-square distance of 40 Å, the thickness of lipid bilayer, is ~2 ns³⁰. This might be the reason for the finding that the endosomal escape efficiencies of the carrier/RNA complexes were highly correlated with the [$\phi_{\Delta} \times Ef$] values without considering the localization of each photosensitizer.

The contribution of ¹O₂ was also indicated using ¹O₂ quenchers. We used four different quenchers, two hydrophilic and two hydrophobic. It was notable that the effects of all the quenchers were very similar despite their different properties. The result that both hydrophilic and hydrophobic quenchers decreased endosomal escape efficiency suggested that the photosensitizers (dyes) of the TatU1A-dye molecules were partly embedded into the endosomal membrane and affected by the hydrophobic quenchers, and partly within the endosomal matrix and thus affected by hydrophilic quenchers as well.

Time-lapse imaging of the endosomal escape indicated that photostimulation induced a pH increase in the endosome followed by endosomal disruption. Imaging of photoinduced endosomal release of macromolecules was also attempted by de Bruin *et al.*³¹. They demonstrated PCI of macromolecules such as dextran labeled with Alexa Fluor 488 and a polyethyleneimine (Alexa Fluor 488)/DNA (Cy5) complex, using meso-tetraphenyl porphyrin disulphonate (TPPS_{2a}) as a photosensitizer, which was not covalently linked to the macromolecules. From this, they clearly showed the release dynamics of the macromolecules, but did not mention any pH increase prior to the endosomal escape. Thus, we believe that the pH increase prior to endosomal escape observed in this study represents a novel finding.

Overall, the results demonstrated in this study suggest that the photoinduced endosomal disruption occurred as follows (Fig. 6): (i) the endosomal membrane was destabilized; (ii) protons were released from the endosome, elevating internal endosome pH; and (iii) the endosomal membrane disrupted and the cargo RNA dispersed from the endosome into the cytosol. The timescale for the photoinduced endosomal disruption (a few seconds to a few minutes) was much longer than the ¹O₂ lifetime (4.2 μs in water and 19 μs in octanol²⁹). Thus, a process(es) must exist after ¹O₂ generation until endosomal disruption that requires a few seconds to a few minutes to complete. This might be a destabilization process induced by membrane lipids damaged by ¹O₂. The hidden process between ¹O₂ generation and endosomal disruption needs to be clarified by future experiments.

Methods

Preparation of TatU1A-dye conjugates. The RNA carrier protein TatU1A, which has a C-terminal Cys residue, was prepared as described previously¹⁵. The purified TatU1A protein and a dye with a thiol-reactive maleimide group were mixed in a buffer containing 50 mM HEPES-KOH (pH 7.5), 100 mM (NH₄)₂SO₄, 150 mM imidazole, and 20% glycerol, and then incubated at 25 °C for 1 h. The dyes used here were Alexa Fluor 594 (Life Technologies, Carlsbad, CA), HiLyte Fluor 594 (AnaSpec, Fremont, CA), Alexa Fluor 633 (Life Technologies), DyLight 633 (Pierce, Rockford, IL), DY 630 (Dyomics, Jena, Germany), Promo Fluor 633 (PromoKine, Heidelberg, Germany), HiLyte Fluor 647 (AnaSpec), Cy5 (GE Healthcare Life Sciences, Tokyo, Japan), and rose bengal, which was synthesized as described in supporting information. The dye-attached TatU1A molecules (TatU1A-dye) were purified in a Centri-Sep spin column (Princeton Separations, Freehold Township, NJ) equilibrated with T buffer [20 mM HEPES-KOH (pH 7.4), 115 mM NaCl, 5.4 mM KCl, 1.8 mM CaCl₂, 0.8 mM MgCl₂, and 13.8 mM glucose]. Protein concentration was determined using a Protein Assay Kit (Bio-Rad, Berkeley, CA). Labeling efficiencies of the carrier proteins were calculated by measuring the absorbance of the respective dyes. In all experiments, labeling efficiencies were adjusted to 40% using separately prepared unlabeled carrier proteins.

FAM-labeled shRNA. A FAM-labeled shRNA was purchased from JBioS (Saitama, Japan). The shRNA sequence used was as follows: 5'- GAU UAU GUC CGG UUA UGU ACA UUG CAC UCC GUA CAU AAC CGG ACA UAA UCdT dT -3' (the U1A binding sequence³² is underlined). This represents a non-specific shRNA in normal mammalian cells, but contains an anti-luciferase sequence. A fluorescent dye (FAM) was attached at the 3'-end of the shRNA. The shRNA was annealed by incubation at 85 °C for 1 min to remove secondary structure followed by slow annealing (−1 °C/s) to 4 °C.

Measurement of the ¹O₂ quantum yields of dyes. The ¹O₂ generation quantum yields of each dye were calculated by comparing the emission intensities of the singlet oxygen photosensitized by each dye at 1270 nm using methylene blue as the standard. In detail, a nanosecond pulsed Nd:YAG laser pumped dye (DCM) laser (500 Hz, pulse width 7 ns, 50 mW) was used for the excitation source, and the emission from a singlet oxygen from the dye was collected by the bundle fiber and detected by the near infrared-photomultiplier tube (NIR-PMT) (H10330B-45, Hamamatsu Photonics K.K., Hamamatsu, Japan) through the band-pass filter (1270 nm or 1200 nm), and recorded by the multi-channel scaler (Nano-Harp 250, Pico-Quant, Berlin, Germany) for 60 s. We measured the decay curves at 1270 nm (singlet oxygen emission) and 1200 nm (background), and subtracted the background from the 1270 nm curves. The emission signal intensity was calculated by accumulating the intensity of the decay curve from 200 ns to 100 μs. The ¹O₂ quantum yields (φ_Δ) of each dye in octanol were calculated by comparing the intensity of the signal of each dye to that of methylene blue in octanol. The intensity of methylene blue in octanol was, in turn, estimated from that in ethanol (0.520)³³ by comparing the ¹O₂ emission intensities sensitized by methylene blue in octanol and in ethanol, which were compensated for light absorption, refractive index, and emission lifetimes. As a result, the ¹O₂ generation quantum yield of methylene blue in octanol was determined as 0.484.

Measurement of fluorescence quantum yield of dyes. The quantum yields of the dye solutions were measured using an absolute photoluminescence quantum yields measurement system, Quantaaurus-QY C11347-11 (Hamamatsu Photonics K.K.). The dye solution (2 mL) was set in a specialized quartz cuvette and excited at a wavelength shorter than the short-edge of the fluorescence spectrum.

Evaluation of the correlation between endosomal escape efficiency and photophysical parameters. The relative efficacy of excitation (Ef) of each photosensitizer, which is relative to that of DY630 (Ef for DY630 = 1), was calculated using the spectrum of the excitation light source (Supplementary Fig. 3) and absorbance spectra of the photosensitizers ($Ef = \frac{\int_{\lambda=541}^{\lambda=592} [\text{absorptivity} \times \text{excitation light strength}] d\lambda}{\int_{\lambda=541}^{\lambda=592} [\text{absorptivity} \times \text{excitation light strength}] d\lambda}$). The values of [φ_Δ × Ef] and [φ × Ef] are linearly correlated to photogenerated ¹O₂ and fluorescence, respectively. The values of [(1 − φ − φ_Δ) × Ef] are considered to be proportional to the photogenerated heat. From these, we generated correlation plots of endosomal escape efficiency versus [φ_Δ × Ef], [φ × Ef], and [(1 − φ − φ_Δ) × Ef].

Cell culture, cell treatment with TatU1A-dye/RNA complexes, and photostimulation. Chinese hamster ovary (CHO) cells were cultured in Ham's F-12 medium (Nacalai Tesque, Kyoto, Japan) supplemented with 10% fetal bovine serum (Nichirei Biosciences, Tokyo, Japan), 100 units/mL penicillin, and 100 μ g/mL streptomycin (Gibco, Invitrogen, Carlsbad, CA). Treatment of the cells with TatU1A-dye/RNA complex was performed as follows: TatU1A-dye (2 μ M) and the FAM-labeled shRNA (200 nM) were mixed in T buffer [20 mM HEPES-KOH (pH 7.4), 115 mM NaCl, 5.4 mM KCl, 1.8 mM CaCl_2 , 0.8 mM MgCl_2 , and 13.8 mM glucose] and incubated at 37 °C for 10 min. CHO cells were grown on a 96-well plate to 70–80% confluence and were treated for 2 h with the TatU1A-dye/RNA complex. After washing, the cells were visualized using a fluorescence microscope (Olympus, Tokyo, Japan). For endosomal escape of the TatU1A-dye/RNA complex, cells were irradiated for 2.6 sec with a 100 W mercury lamp (Olympus U-LH100HG) passed through the WIY mirror unit, a 40 \times objective lens (Olympus 40 \times /0.60 Ph2 LUCPlanFLN), and a 12% ND filter. This light source obtained with the WIY mirror unit provided peak light intensity at 580 nm. By this irradiation method, the light dose to the cells was 10 J/cm². The photoinduced endosomal escape efficiencies of the FAM-labeled RNA with each TatU1A-dye were calculated by counting the number of cells in which FAM fluorescence was dispersed within the cytosol after photostimulation (N_F) and the total cell number (N_T) using FAM fluorescence and phase-contrast images from the same area. The endosomal escape efficiency was defined as $N_F / N_T \times 100$ (%).

Influences of ¹O₂ quenchers toward photo-dependent endosomal escape of the TatU1A-dye/RNA complexes. Cells were treated with TatU1A-Alexa633/RNA complexes as described above. One of the ¹O₂ quenchers listed below was added to the cells at the following time points; (i) at the same time as treatment with the complex, or (ii) after treatment with the complex. The ¹O₂ quenchers used here were L-histidine (final concentration 25 mM for incubation of the cells), NaN₃ (25 mM), crocetin (50 μ M), and α -tocopherol (50 μ M).

Imaging of photoinduced endosomal disruption by fluorescence microscopy. CHO cells were seeded on a 35-mm glass-bottom dish (MatTek, P35G-1.5-10-C) at a concentration of 2×10^4 cells per dish (the volume of medium was 150 μ L per dish). On the next day, TatU1A-Alexa546/FAM-shRNA complexes prepared as described above in 100 μ L T buffer were loaded onto the cells and incubated for 2 h in a CO₂ incubator. The cells were washed with 150 μ L T buffer twice and then observed in T buffer. Live cell imaging was performed using a DeltaVision microscope system (Applied Precision) placed in a temperature controlled room (37 °C)³⁴. Light irradiation and subsequent time-lapse imaging were performed through the Olympus UApO/340 oil-immersion objective lens (40 \times , NA 0.65-1.35) at the NA value of =0.65. For the excitation of Alexa546, light at the wavelength of 529–556 nm (InsightSSI) was used at an irradiance of 1.47 W/cm² for 6.8 s (approximately 10 J/cm²). Immediately after the irradiation, time-lapse images were obtained every 5 s. For measuring the fluorescence intensities at endosomal dots in the time-lapse images, ImageJ software (National Institutes of Health, Bethesda, MD) equipped with the SpotTracker 2D plug-in was used.

References

1. Fu, A., Tang, R., Hardie, J., Farkas, M. E. & Rotello, V. M. Promises and pitfalls of intracellular delivery of proteins. *Bioconjug. Chem.* **25**, 1602–1608 (2014).
2. Seth, S., Johns, R. & Templin, M. V. Delivery and biodistribution of siRNA for cancer therapy: challenges and future prospects. *Ther. Deliv.* **3**, 245–261 (2012).
3. Theodossiou, T. A., Goncalves, A. R., Yannakopoulou, K., Skarpen, E. & Berg, K. Photochemical internalization of tamoxifens transported by a “Trojan-horse” nanoconjugate into breast-cancer cell lines. *Angew. Chem. Int. Ed. Engl.* **54**, 4885–4889 (2015).
4. Bostad, M. *et al.* Light-controlled endosomal escape of the novel CD133-targeting immunotoxin AC133-saporin by photochemical internalization - A minimally invasive cancer stem cell-targeting strategy. *J. Control. Release* **206**, 37–48 (2015).
5. Weyergang, A. *et al.* Photochemical internalization augments tumor vascular cytotoxicity and specificity of VEGF(121)/rGel fusion toxin. *J. Control. Release* **180**, 1–9 (2014).
6. Selbo, P. K. *et al.* Photochemical internalization provides time- and space-controlled endolysosomal escape of therapeutic molecules. *J. Control. Release* **148**, 2–12 (2010).
7. Berg, K. *et al.* Photochemical internalization: a novel technology for delivery of macromolecules into cytosol. *Cancer Res.* **59**, 1180–1183 (1999).
8. Boe, S. L. & Hovig, E. Enhancing nucleic acid delivery by photochemical internalization. *Ther. Deliv.* **4**, 1125–1140 (2013).
9. Meerovich, I., Muthukrishnan, N., Johnson, G. A., Erazo-Oliveras, A. & Pellois, J. P. Photodamage of lipid bilayers by irradiation of a fluorescently labeled cell-penetrating peptide. *Biochim. Biophys. Acta* **1840**, 507–515 (2014).
10. Wang, J. T., Giuntini, F., Eggleston, I. M., Bown, S. G. & MacRobert, A. J. Photochemical internalisation of a macromolecular protein toxin using a cell penetrating peptide-photosensitizer conjugate. *J. Control. Release* **157**, 305–313 (2012).
11. Muthukrishnan, N., Johnson, G. A., Lim, J., Simanek, E. E. & Pellois, J. P. TAT-mediated photochemical internalization results in cell killing by causing the release of calcium into the cytosol of cells. *Biochim. Biophys. Acta* **1820**, 1734–1743 (2012).
12. Srinivasan, D. *et al.* Conjugation to the cell-penetrating peptide TAT potentiates the photodynamic effect of carboxytetramethylrhodamine. *PLoS One* **6**, e17732 (2011).
13. Matsushita-Ishiodori, Y., Kuwabara, R., Sakakoshi, H., Endoh, T. & Ohtsuki, T. Photosensitizing carrier proteins for photoinducible RNA interference. *Bioconjug. Chem.* **22**, 2222–2226 (2011).
14. Endoh, T., Sisido, M. & Ohtsuki, T. Spatial regulation of specific gene expression through photoactivation of RNAi. *J. Control. Release* **137**, 241–245 (2009).
15. Endoh, T., Sisido, M. & Ohtsuki, T. Cellular siRNA delivery mediated by a cell-permeant RNA-binding protein and photoinduced RNA interference. *Bioconjug. Chem.* **19**, 1017–1024 (2008).
16. Bostad, M. *et al.* Photochemical internalization (PCI) of immunotoxins targeting CD133 is specific and highly potent at femtomolar levels in cells with cancer stem cell properties. *J. Control. Release* **168**, 317–326 (2013).
17. Oliveira, S., Fretz, M. M., Hogset, A., Storm, G. & Schifferers, R. M. Photochemical internalization enhances silencing of epidermal growth factor receptor through improved endosomal escape of siRNA. *Biochim. Biophys. Acta* **1768**, 1211–1217 (2007).
18. Boe, S., Longva, A. S. & Hovig, E. Photochemically induced gene silencing using small interfering RNA molecules in combination with lipid carriers. *Oligonucleotides* **17**, 166–173 (2007).
19. Gandin, E., Lion, Y. & Van de Vorst, A. Quantum yield of singlet oxygen production by xanthene derivatives. *Photochem. Photobiol.* **37**, 271–278 (1983).
20. Kobayashi, S. *et al.* Artificial induction of autophagy around polystyrene beads in nonphagocytic cells. *Autophagy* **6**, 36–45 (2010).

21. Kobayashi, S. *et al.* BAF is a cytosolic DNA sensor that leads to exogenous DNA avoiding autophagy. *Proc. Natl. Acad. Sci. USA* **112**, 7027–7032 (2015).
22. Fujita, N. *et al.* Recruitment of the autophagic machinery to endosomes during infection is mediated by ubiquitin. *J. Cell Biol.* **203**, 115–128 (2013).
23. Weyergang, A., Selbo, P. K. & Berg, K. Photochemically stimulated drug delivery increases the cytotoxicity and specificity of EGF-saporin. *J. Control. Release* **111**, 165–173 (2006).
24. Shiraiishi, T. & Nielsen, P. E. Photochemically enhanced cellular delivery of cell penetrating peptide-PNA conjugates. *FEBS Lett.* **580**, 1451–1456 (2006).
25. Ndoye, A. *et al.* Eradication of p53-mutated head and neck squamous cell carcinoma xenografts using nonviral p53 gene therapy and photochemical internalization. *Mol. Ther.* **13**, 1156–1162 (2006).
26. Woodhams, J. *et al.* Intracellular re-localisation by photochemical internalisation enhances the cytotoxic effect of gelonin—quantitative studies in normal rat liver. *J. Control. Release* **142**, 347–353 (2009).
27. Berg, K. *et al.* Disulfonated tetraphenyl chlorin (TPCS2a), a novel photosensitizer developed for clinical utilization of photochemical internalization. *Photochem. Photobiol. Sci.* **10**, 1637–1651 (2011).
28. Ehrenberg, B., Anderson, J. L. & Foote, C. S. Kinetics and yield of singlet oxygen photosensitized by hypericin in organic and biological media. *Photochem. Photobiol.* **68**, 135–140 (1998).
29. Rodgers, M. A. Time resolved studies of 1.27 micron luminescence from singlet oxygen generated in homogeneous and microheterogeneous fluids. *Photochem. Photobiol.* **37**, 99–103 (1983).
30. Bronshtein, I. *et al.* Porphyrin depth in lipid bilayers as determined by iodide and parallax fluorescence quenching methods and its effect on photosensitizing efficiency. *Biophys. J.* **87**, 1155–1164 (2004).
31. de Bruin, K. G. *et al.* Dynamics of photoinduced endosomal release of polyplexes. *J. Control. Release* **130**, 175–182 (2008).
32. Hall, K. B. & Stump, W. T. Interaction of N-terminal domain of U1A protein with an RNA stem/loop. *Nucleic Acids Res.* **20**, 4283–4290 (1992).
33. Nemoto, M., Kokubun, H. & Koizumi, M. Determination of the S*–T Transition Probabilities of Some Xanthene and Thiazine Dyes on the Basis of the T-Energy Transfer. I. Experiment in Ethanol Solutions. *Bull. Chem. Soc. Jpn.* **42**, 1223–1230 (1969).
34. Haraguchi, T. *et al.* BAF is required for emerlin assembly into the reforming nuclear envelope. *J. Cell Sci.* **114**, 4575–4585 (2001).

Acknowledgements

We thank Y. Inaba (Okayama University) for the fluorescence measurements of shRNA-FAM and Alexa546. This work was supported by a Grant-in-Aid for Scientific Research (Grant number 25282232 to T.O.) and Grants-in-Aid for Scientific Research on Innovative Areas “Nanomedicine Molecular Science” (26107711 to T.O. and 26107710 to E.N.).

Author Contributions

T.O. designed the experiments and wrote the paper. S.O., S.M., K.M. and K.H. measured $^1\text{O}_2$ and fluorescence quantum yields. S.K., S.M. and T.H. performed the time lapse imaging. E.N. synthesized rose bengal-maleimide. S.M. and K.M. primarily performed experiments with the guidance of T.O. and K.W.

Additional Information

Supplementary information accompanies this paper at <http://www.nature.com/srep>

Competing financial interests: The authors declare no competing financial interests.

How to cite this article: Ohtsuki, T. *et al.* The molecular mechanism of photochemical internalization of cell penetrating peptide-cargo-photosensitizer conjugates. *Sci. Rep.* **5**, 18577; doi: 10.1038/srep18577 (2015).



This work is licensed under a Creative Commons Attribution 4.0 International License. The images or other third party material in this article are included in the article’s Creative Commons license, unless indicated otherwise in the credit line; if the material is not included under the Creative Commons license, users will need to obtain permission from the license holder to reproduce the material. To view a copy of this license, visit <http://creativecommons.org/licenses/by/4.0/>